# KLOE-2 Collaboration - LNF Group

D. Babusci, C. Bloise, F. Bossi, G. Capon (Ass.), P. Ciambrone, F. Curciarello (PostDoc),
E. De Lucia (Resp.), A. De Santis, P. De Simone, A. Di Cicco (PostDoc),
D. Domenici,G. Fortugno (Tec.), S. Giovannella, X. Kang (PostDoc), M. Martini (Ass)*,
S. Miscetti, D. Moricciani, P. Santangelo, F. Sborzacchi (Tec.).

*Also Dipartimento di Scienze e Tecnologie applicate,"Guglielmo Marconi" University, Rome, Italy*

## 1 Introduction

KLOE and KLOE-2 data set of about $2.4\times10^{10}$ $\phi$-meson produced represents the largest sample ever collected at the $\phi(1020)$ meson peak at $e^+e^-$ colliders. $K_S$ and $\eta$ meson rare decays as well as on kaon interferometry, fundamental symmetry tests and physics beyond the Standard Model, are the focus of the physics program which includes also searches for new exotic particles that could constitute the dark matter. Present activities are mainly focused on data reconstruction and analysis towards precise measurements in both kaon and hadron sectors. The final round of data reconstruction started in March 2020 and a full MC data sample with Luminosity Scale Factor (LSF) = 1 was produced and reconstructed, exploiting the features of the experiment CED expanded and renewed for Data Consolidation. Also the long-term plan for Data Preservation, established and started last year, proceeded smoothly in 2020.

KLOE-2 collaboration published the first measurement ever of the $K_S \to \pi\mu\nu$ branching ratio [1] allowing an independent determination of the CKM matrix element $|V_{us}|$ and the first test of the lepton-flavour universality with $K_S$ decays and the published the final result on the $\eta \to \pi^+\pi^-$ upper limit [2] on the nature of CP violation in strong interactions. Latest physics results achieved in 2020 are: i) preliminary results on the direct test of T and CPT symmetries in neutral kaon transitions, ii) preliminary results on the search for decoherence and CPTV in $\phi \to K_S K_L \to \pi^+\pi^-\pi^+\pi^-$ using 1.7 fb$^{-1}$, iii) the statistical evidence of correlated coincidence events between the HET tagger station and the central calorimeter [3] in the search for candidates of single-$\pi^0$ production from $\gamma\gamma$ scattering with 1.5 fb$^{-1}$, iv) the clear signal evidence in the 4-$\gamma$ invariant mass distribution of the 5 prompt photons sample from $\eta \to \pi^0\gamma\gamma$ decay, a $\chi_{PT}$ golden mode sensitive to O(p$^6$) and v) clear signal peaks from $\phi \to \eta \to \pi^+\pi^-/\eta \to \mu^+\mu^-$ decays vi) the final invariant mass distributions from $\phi \to \eta B \to \eta\pi^0\gamma$ and $\eta \to B\gamma \to \pi^0\gamma\gamma$ decays to search for the B-boson, a leptophobic mediator between the dark sector and the Standard Model particles [4].

## 2 Data Reconstruction and MC simulation

The final round of data processing was started in March 2020 with a reconstruction average rate of about 20 pb$^{-1}$/day and 30 pb$^{-1}$/day peak rate, similarly to the previous data processing campaign. A total of 2.5 fb$^{-1}$ were reconstructed during 2020 with the improved version of the official reconstruction software, which includes more accurate detector material description and revised algorithms to improve both signal event yield and effective background discrimination.
With the first reconstructed fb$^{-1}$, the KLOE-2 collaboration assessed data quality and performance of the final reconstruction software, by analyzing selected reactions and comparing them to the previous reconstructed data. Along with the reconstruction process and following the established Data Preservation long-term plan, a sample of ROOT output files was produced to be used in the aforementioned data quality studies.

## 3 CED

KLOE CED consolidation activities, started in 2019, continued during 2020 together with the usual tasks. *Data Preservation* proceeded smoothly, moving the precious KLOE and KLOE-2 raw data from both the old IBM3494 and new TS4500 tape libraries to a disaster recovery LTO tape library. About 69% of the whole dataset has been copied.
The GPFS migration from the AFS protocol was completed making the whole infrastructure stronger. Presently GPFS protocol moves data through the entire CPU-cluster reaching the highest rate in data moving we have ever had with the sustained throughput level of 8 Gbyte per second for each disk array available on Fiber Channel network. The disk arrays available on our network are now three and the total amount of storage slightly exceeds one Petabyte. This high throughput rate deploys to our users the possibility to elaborate their data faster and reliably. Additional cartridges were also mounted in the main library, 300 cartridges with 10 TB capacity each, thus allowing to start the copy of the entire dataset stored in the old library into the new library. The library now has 11 Pbyte available. Fig.1 shows the usage plan for the new tape library, including the disaster recovery service for the PADME experiment. Both copying tasks involving this tape library, to the LTO and from the old IBM3494 tape libraries, should be completed by the end of the year.

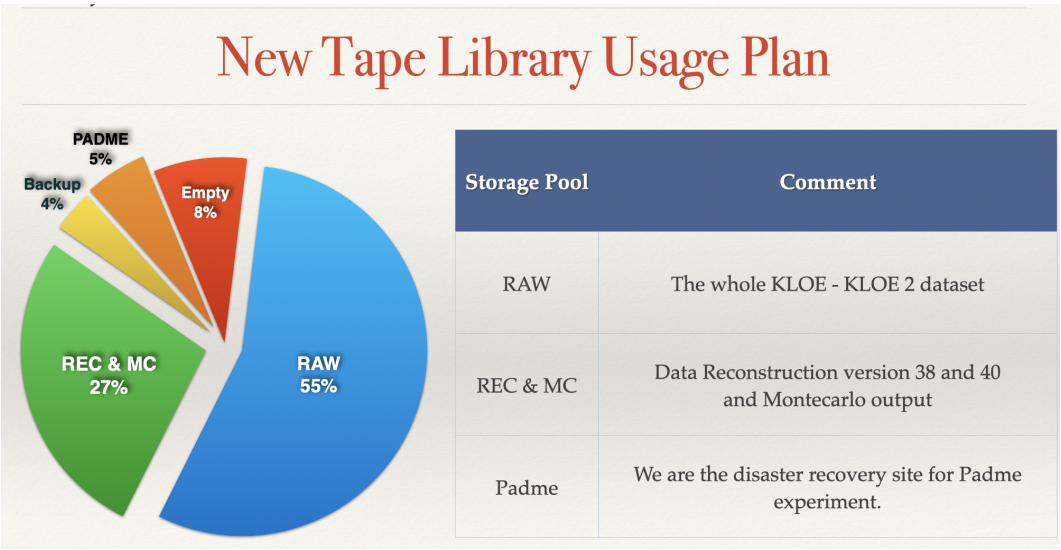


Figure 1: New Tape Library usage plan.

A new job submission system was put in place to substitute the previous one compatible with AFS file systems. The old procedure never missed a single job submission, even though AFS has always introduced a huge slow down in managing the system. Presently the job submission carried by GPFS file servers is able to manage and dispatch more efficiently the daily load generated by users and to carry on the task even with thousands jobs enqueued. After the change, happened at the beginning of December, the cluster has already dispatched and accomplished more than one hundred thousand different jobs. Fig.2 left shows the fiber channel total throughput with and without AFS protocol. Both size and speed of the disk arrays are shown in Fig.2 right.
The structure of KLOE CED has become more compact and efficient, reliable and reactive to the user's requests with the GPFS as a new data distribution centre. Every client has a multipath channel to read and write data guaranteed as speed, to reduce the wait time for every IO operation.

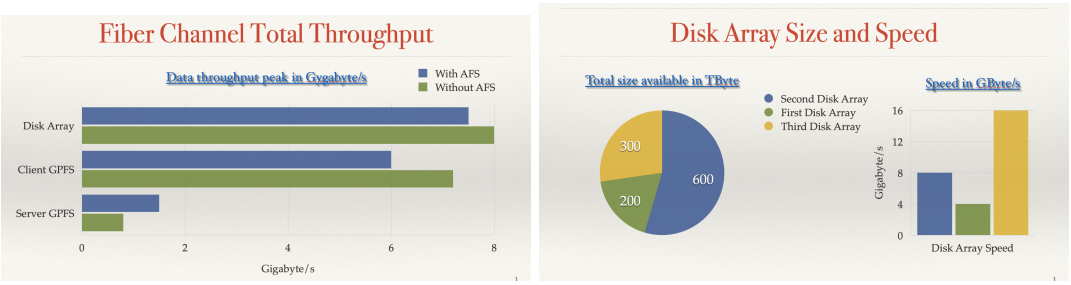


Figure 2: Throughput for each disk array no longer working in AFS and GPFS protocol simultaneously but only in GPFS protocol (left). Size and speed of each disk array working on KLOE fiber channel network under GPFS protocol (right).

The increase in terms of speed is the cornerstone of the new architecture, started in 2019 and now completed. Concluding, every task increased its own efficiency with the storage area network and beside, we have created a redundant distribution system for the data which led to zero the number of jobs slowed down due to network congestion or because there are a lot of requests to the same AFS volume locking the file requests for new jobs.

## 4 Physics achievements

The integrated luminosity collected by KLOE and KLOE-2 experiments represents a unique data sample which is very rich in physics. It will allow the deep investigation and exploitation of one of the most peculiar characters of neutral kaons produced at a $\phi$-factory, the entanglement, specific to two neutral kaon systems in a coherent quantum state, that will be studied and tested with unprecedented statistics together with light mesons. Latest achievements will be discussed in following sections.

### 4.1 Direct test of T and CPT symmetries in neutral kaon transitions

The comparison of neutral meson transition rates between flavour and CP eigenstates allows direct and model independent tests of time-reversal T and CPT symmetries [5] to be performed. To identify the initial state of a particle transition by the decay of its entangled partner quantum entangled kaon pairs are used. The final state instead is tagged by semileptonic and hadronic decays into two and three pions.

T-violation can be tested through the following ratios of the rates of two classes of processes identified in the dataset $K_S K_L \to \pi^{\pm} e^{\mp} \nu, 3\pi^0$ and $K_S K_L \to \pi^+\pi^-, \pi^{\pm} e^{\mp} \nu$:

$$\mathrm{R}_2(\Delta t) = \frac{\mathrm{P}[\mathrm{K}^0(0) \to \mathrm{K}_-(\Delta t)]}{\mathrm{P}[\mathrm{K}_-(0) \to \mathrm{K}^0(\Delta t)]} \sim \frac{\mathrm{I}(\pi^+ e^- \bar{\nu}, 3\pi^0; \Delta t)}{\mathrm{I}(\pi^+\pi^-, \pi^- e^+ \nu; \Delta t)}, \tag{1}$$

$$\mathrm{R}_4(\Delta t) = \frac{\mathrm{P}[\bar{\mathrm{K}}^0(0) \to \mathrm{K}_-(\Delta t)]}{\mathrm{P}[\mathrm{K}_-(0) \to \bar{\mathrm{K}}^0(\Delta t)]} \sim \frac{\mathrm{I}(\pi^- e^+ \nu, 3\pi^0; \Delta t)}{\mathrm{I}(\pi^+\pi^-, \pi^+ e^- \bar{\nu}; \Delta t)}, \tag{2}$$

with $\mathrm{I}(f_1, f_2; \Delta t)$ denoting the number of recorded events characterized by a time-ordered pair of kaon decays $f_1$ and $f_2$ separated by an interval of proper kaon decay times $\Delta t$ [5]. A deviation from unity of the asymptotic level of these ratios at large transition time values would be a T-violation manifestation.

CPT symmetry can also be tested and in this case the determination of the asymptotic level of this double ratio is used:

$$\frac{R_2^{CPT}}{R_4^{CPT}} = \frac{\mathrm{P[K^0(0) \to K_-(\Delta t)]/P[K_-(0) \to \bar{K}^0(\Delta t)]}}{\mathrm{P[\bar{K}^0 \to K_-(\Delta t)]/P[K_-(0) \to K^0(\Delta t)]}} \overset{\Delta t \gg \tau_S}{=} 1 - 8Re(\delta) - 8Re(x_-), \qquad (3)$$

with $\delta$ and $x_-$ being the parameters violating CPT symmetry in $\mathrm{K^0\bar{K}^0}$ mixing and the $\Delta S = \Delta Q$ rule, respectively. This double ratio represents a robust CPT-violation sensitive observable [5] which has never been measured to date. A percent level accuracy was obtained on the double ratio measurement with 1.7 $\mathrm{fb^{-1}}$ KLOE data sample. The results in Fig.3 were shown at the $60^{th}$ LNF Scientific Committee meeting.

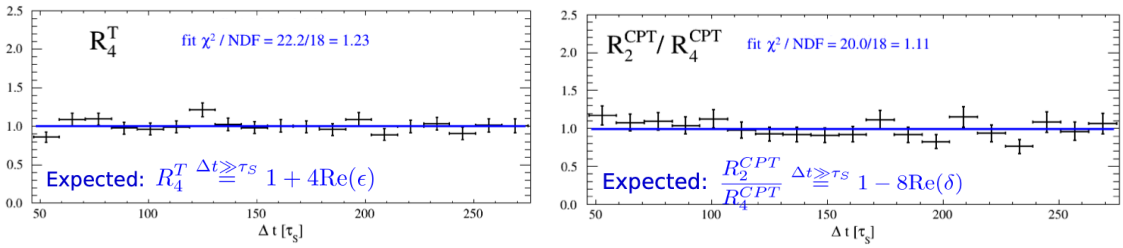


Figure 3: T-violation sensitive ratio $R_4^T$ (left) and CPT-violation sensitive double ratio $R_2^{CPT}/R_4^{CPT}$ (right) distributions.

The final evaluation of systematic uncertainties is ongoing. Adding KLOE-2 data set, the accuracy is expected to be reduced down to the $10^{-3}$ level of precision.

### 4.2 Search for decoherence and CPT violation in $\phi \to K_S K_L \to \pi^+\pi^-\pi^+\pi^-$

The $\phi$-meson decay into neutral kaons produces one of the most intriguing system in the particle physics landscape: an entangled pair of massive particles. According to the $\phi$-meson quantum numbers, the produced neutral kaon system has to be fully antisymmetric implying a complete cancellation of the combined decay amplitudes in the same final state for the two kaons. This peculiar behaviour is a powerful test bench for quantum physics and it's implication on the time evolution of the system. By considering the decay amplitude as a function of the decay time difference for the two kaons in the $\pi^+\pi^-$ final state, a fully destructive interference is expected, and indeed observed, for equal decay time (Fig. 4).

Assuming a violation of the standard quantum-mechanical time evolution of the system, it is possible to introduce a fully phenomenological approach by inserting an extra parameter accounting for the deviation from the expected behavior. This term, known a "decoherence" parameter, appears in the amplitude equation with the neutral kaon state projected alongside the flavor eigenstate [6]:

$$I(\pi^+\pi^-,\pi^+\pi^-;\Delta t) = \frac{N}{2}\Big[\big|\langle\pi^+\pi^-,\pi^+\pi^-|K^0\bar{K}^0(\Delta t)\rangle\big|^2 + \big|\langle\pi^+\pi^-,\pi^+\pi^-|\bar{K}^0K^0(\Delta t)\rangle\big|^2 \qquad (4)$$

$$-2(1-\zeta_{0\bar{0}})\Re e(\langle\pi^+\pi^-,\pi^+\pi^-|K^0\bar{K}^0(\Delta t)\rangle\langle\pi^+\pi^-,\pi^+\pi^-|K^0\bar{K}^0(\Delta t)\rangle^*)\Big]$$

The decoherence parameter can be introduced also using the mass eingestate representation. Other mechanisms could be assumed, among these are the ones relating the decoherence of the system time evolution to CPT violation through quantum gravity effects. In this case other parameters

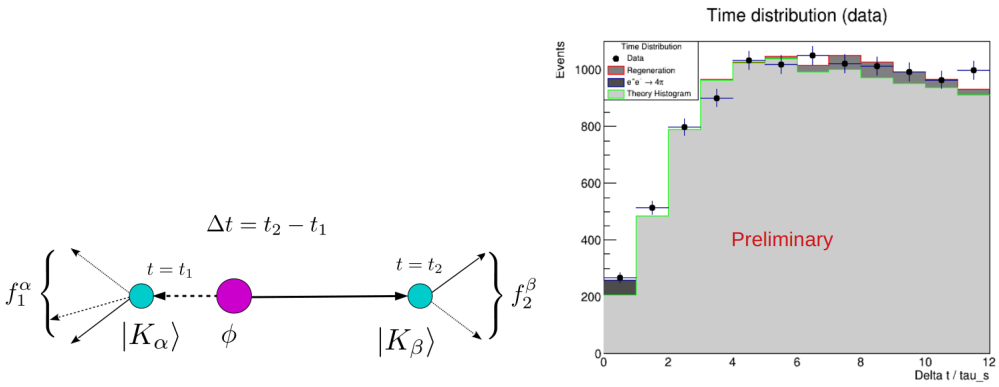


Figure 4: Left: sketch of the time evolution of the kaon system: the first decay ($f_1^\alpha$) at time $t_1$ and the second decay ($f_2^\beta$) observed at time $t_2$. The entanglement between the two kaons forbids same decay at the same time ($\Delta t = 0$). Right: distribution of the time difference between same decay ($\pi^+\pi^-$) of the two kaons for 1.7 $fb^{-1}$ of data collected by KLOE. Observed distributions (dots) is compared with Monte-Carlo prediction (shaded histograms). The effect of resolution on the reconstruction of the decay vertices can be appreciated in the first bins, where the effect of the quantum correlation causes a complete drop to zero of the theoretical distribution.

are introduced to describe the modified evolution time of the entangled kaon system [7] or the modification of the initial state [8].

Present activity is using 1.7 fb$^{-1}$ KLOE data and represents the natural continuation of the previous analysis performed using a small sample of 380 $pb^-1$ KLOE data [9]. A revised treatment of the data has been used allowing an increased resolution in the decay time measurement [10] to be achieved. Further improvement on the description of the kaon regeneration on the DA$\phi$NE beam pipe and a more detailed treatment of the four-pion non resonant production have been also applied. Preliminary results presented at the $60^{th}$ LNF Scientific Committee meeting show that the statistical uncertainty on the decoherence parameters is reduced by half with the whole KLOE data sample. The effort is now focused on the systematical uncertainty evaluation.

### 4.3 $\eta \to \pi^0\gamma\gamma$

The $\eta \to \pi^0\gamma\gamma$ decay is an important test of $\chi_{PT}$ because of its sensitivity to $p^6$ on both the branching ratio (BR) and the $M_{\gamma\gamma}$ spectrum. [11, 12] The most accurate determination of the BR has been obtained by the Crystal Ball experiment at MAMI, [13] which measured $BR(\eta \to \pi^0\gamma\gamma) = (25.2 \pm 2.5) \times 10^{-5}$. A preliminary KLOE measurement, [14] based on 70 signal events, provided a 4 $\sigma$'s lower value: $BR(\eta \to \pi^0\gamma\gamma) = (8.4 \pm 2.7_{\rm stat} \pm 1.4_{\rm syst}) \times 10^{-5}$.

A new KLOE-2 analysis is in progress on an about four times larger data sample, 1.7 fb$^{-1}$. Background is largely dominated by $\eta \to 3\pi^0$ events, with lost or merged photons. The various background contributions are extracted with a fit to the cluster energy with Monte Carlo shapes, after having improved resolutions by means of a kinematic fit. A TMVA-BDT Multivariate Analysis based on cluster shapes reduces events with merged photon clusters. In order to reduce systematic effects, the number of signal events is normalized to the fully neutral $\eta \to \pi^0\pi^0\pi^0$ sample. Data-MC comparison of the six-photons' invariant mass, reported in Fig. 5 left, shows a good agreement for the normalization sample. At the end of the analysis chain, the overall analysis efficiency for signal is $\sim 20\%$. A signal excess is clearly visible on top of the dominant $\eta \to \pi^0\pi^0\pi^0$ background

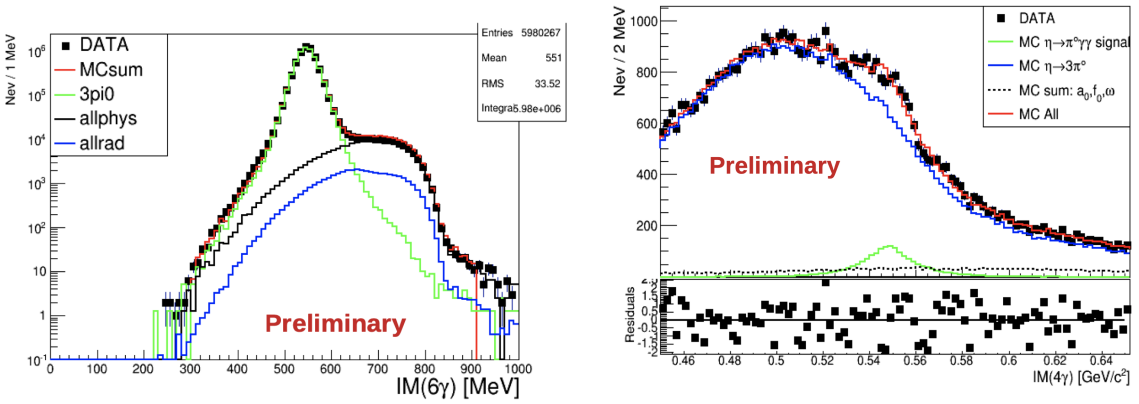


Figure 5: Data-MC comparison for $\eta \to \pi^0\gamma\gamma$ analysis. Invariant mass distribution of $\eta \to 3\pi^0$ normalization sample (left) and invariant mass distribution of the four photons assigned to $\eta$ (right). Dots are data, while the different MC contributions are reported as solid lines. On the bottom, data-MC residuals are shown.

(Fig. 5 right), with a signal to background ratio of S/B $\sim 0.1$ in the signal region, and a number of signal events of $\sim 1,700$. The statistical uncertainty has been reduced by a factor of three with respect to the previous preliminary KLOE measurement. Consistency checks of different fitting strategies and systematic uncertainty evaluation are still ongoing.

### 4.4 $\phi \to \eta \to \pi^+\pi^-/\eta \to \mu^+\mu^-$

In the vector-meson dominance (VMD) model, $e^+e^- \to \eta\pi^+\pi^-$ is proceeded by $\rho$ resonances and mainly via $\rho\eta$ intermediate state, which contributes to the total hadronic cross section. The cross section of this process was measured by BaBar, CMD-2 and SND collaborations in the energy region above 1.2 GeV [15]. With the $e^+e^-$ collision data collected at $\phi$-meson peak by KLOE/KLOE-2 detector, it's possible to study this process in the low energy region. The decay $\phi \to \eta\pi^+\pi^-$ is double suppressed by $G-$parity and the OZI rule, which gives this decay specific interest. The CMD-2 Collaboration set the upper limit of $1.8 \times 10^{-5}$ at 90% of CL [16]. The VMD model predicts the branching ratio to be $0.35 \times 10^{-6}$, which is achievable with KLOE data. The same data sample can be also used to search for the Dalitz decay $\phi \to \eta\mu^+\mu^-$, which has an upper limit of $0.94 \times 10^{-5}$ [16] also set by CMD-2.

A first 760 $pb^{-1}$ data sample has been used to tune the analysis of $\phi \to \eta\pi^+\pi^-$ and $\phi \to \eta\mu^+\mu^-$ with $\eta \to \gamma\gamma$ or $\eta \to \pi^0\pi^0\pi^0$. The candidate events are selected by requiring two charged secondary tracks with opposite curvatures and two or six prompt clusters. Tracks are assumed to come from charged pions or muons and a vertex is required to be reconstructed in a cylindrical volume with dimension $\rho_{vtx} < 4$ cm and $|z_{vtx}| < 10$ cm. Prompt clusters are defined by requiring their Time-of-Flight $T_{clu}$ to satisfy $|T_{clu} - R_{clu}/c| < min(2, 5\sigma_t)$ ns, where $R_{clu}$ is the distance from the position of the cluster to the interaction point, $c$ is the speed of light and $\sigma_t$ is the calorimeter time resolution at the cluster energy. Energy deposits of clusters in the calorimeter are required to be larger than 15 MeV and the angular acceptance is $|cos\theta| < 0.92$. To suppress background contamination, kinematic fits are performed respectively for $\pi^+\pi^-\gamma\gamma$, $\mu^+\mu^-\gamma\gamma$, $\pi^+\pi^-6\gamma$, and $\mu^+\mu^-6\gamma$ hypothesis, by enforcing energy-momentum conservation and the time conservation for each photon. After proper cuts on the $\chi^2$ of the kinematic fits, the invariant mass of $\gamma\gamma$ and $6\gamma$ are shown in Fig. 6. Clear peaks are observed around the $\eta$-meson signal mass in both spectra, which

correspond to clear $\eta\pi^+\pi^-$ and $\eta\mu^+\mu^-$ decay signals with both $\eta \to \gamma\gamma$ and $\eta \to 6\gamma$ channels.

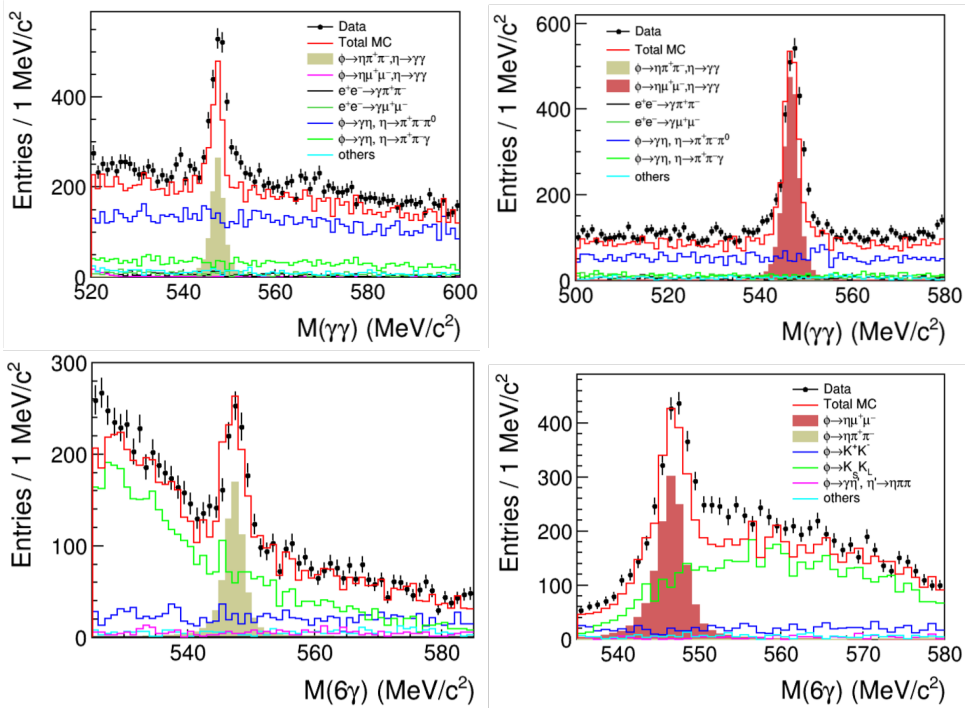


Figure 6: Upper panel: Invariant mass of $\gamma\gamma$ for $\gamma\gamma\pi^+\pi^-$ (left) and $\gamma\gamma\mu^+\mu^-$ (right). Bottom panel: Invariant mass of $6\gamma$ for $6\gamma\pi^+\pi^-$ (left) and $6\gamma\mu^+\mu^-$ (right).

These results were shown at the open session of the $60^{th}$ LNF Scientific Committee meeting. With KLOE/KLOE-2 data samples, the branching ratio of $\phi \to \eta\pi^+\pi^-$ and $\phi \to \eta\mu^+\mu^-$ dacays will be measured for the first time and the potential of the cross section measurement of $e^+e^- \to \eta\pi^+\pi^-$ will be validated.

### 4.5 $\pi^0$ production from $\gamma\gamma$ scattering

The precision measurement of the $\pi^0 \to \gamma\gamma$ width would give insight into low-energy QCD dynamics. To achieve the $\mathcal{O}(1\%)$ precision needed to test theory predictions, KLOE-2 exploits the $\pi^0$ production through $\gamma\gamma$ fusion in the $e^+e^- \to e^+e^-\gamma^*\gamma^* \to e^+e^-\pi^0$ reaction [17]. To reduce the background from $\phi$-meson decays, two High Energy Tagger (HET) stations [18] have been used to detect off-energy leptons scattered in the final state. The HET detectors, made up of 28 plastic scintillators, are installed in roman pots just at the exit of the DA$\Phi$NE dipole magnets, 11 m away from the interaction point (IP), both on positron and electron sides. HET scintillators are placed at difference distances from the beam line, scintillators from 1 to 14 are on the horizontal plane of the machine while scintillators from 15 to 28 are displaced by a maximum of 2.8 mm in step on 200 $\mu$m, to account for combined effects of the KLOE magnetic field and DA$\Phi$NE compensators on the off-energy particles.

The HET acquisition system has been designed to register more than two turns of the machine. Therefore, the time window of the HET data acquisition is wider than KLOE one ($\sim 250$ ns) and varies from 660 to 970 ns. $\gamma\gamma \to \pi^0$ signal is expected in the coincidence window between HET and

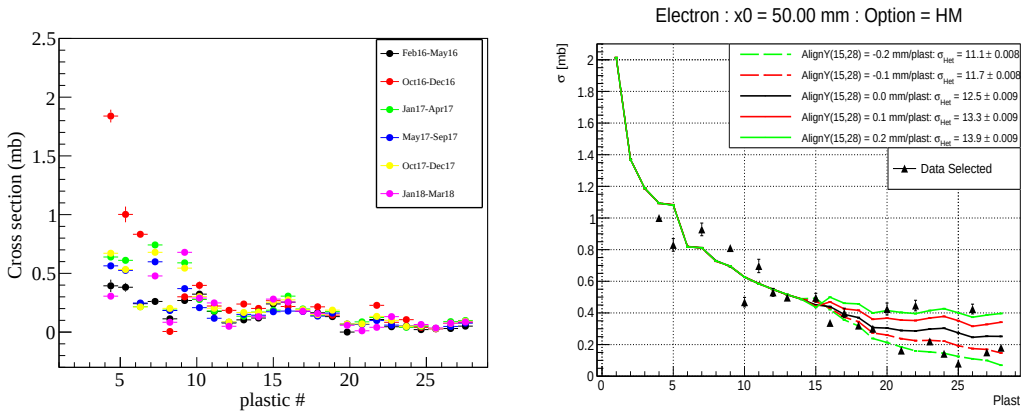


Figure 7: Left panel: effective low-angle radiative Bhabha cross section per plastic as measured by the electron station in different periods of the 2016, 2017 and 2018 data taking. Right panel: low-angle radiative Bhabha cross section obtained from the Bbbrem simulation [19] for different displacements of the HET plastics on the $Y$ axis; the simulation outcomes (colored lines) are compared with measurements corrected for the efficiency (black triangles).

KLOE while the remaining buffer depth, acquired together with the coincidence sample, is used to evaluate the amount of uncorrelated time coincidences between the two detectors (accidentals).

The accidental counting rate is dominated by low-angle radiative Bhabha scattering and we use the effective cross-section, as a function of the data-taking period, to measure the detector acceptance×efficiency and for data quality.

Figure 7 left panel shows the effective low-angle radiative Bhabha cross section per plastic as measured by the electron station in different data-taking periods. An effective total average cross section of 2.5 $\pm$0.04 mb has been measured for plastics from 10 to 28 with data acquired between 2016 and 2018. HET scintillators closer to the beam show large fluctuations mainly related to an higher intra-bunch scattering background. In Figure 7 right panel, the comparison between the low-angle radiative Bhabha cross section from Bbbrem simulation [19], for different Y displacements of the HET scintillators, and the measurements corrected for the efficiency is reported. The "tuning" of $Y$ HET plastic positions in the simulation and the comparison with measured cross section allow to infer the actual HET acceptance.

For the $\pi^0$ search a sub-set of HET plastic scintillators has been used, chosen for their operational stability over time scale of years. Candidates of single-$\pi^0$ production from $\gamma\gamma$ scattering have been pre-filtered recording information on the hit in the tagger, on the trigger signal, the DA$\Phi$NE operational parameters, clusters and tracks reconstructed in the KLOE central detector. Data are classified as single-arm (SA) or double-arm (DA) events. DA events are selected requiring the time coincidence of the two HET stations within 12 ns, while for SA events, we selected hits in one HET station and at least one bunch in the KLOE central detector associated with only 2 clusters in the calorimeter. Very loose kinematic cuts are applied to this sample. Statistical evidence of correlated coincidence events between the tagger station and the KLOE calorimeter has been observed on a sample of 1.5 fb$^{-1}$ (1/2 of the reconstructed KLOE-2 statistics), on the electron side, with a precision of 10% in a KLOE-HET coincidence window of 4 bunches.

Fig. 8 shows the results of the simultaneous fits of the KLOE-HET coincidence sample (A+ sample) in the main independent $\pi^0$ kinematic variables. The A+ sample is constituted by a large amount of accidentals (A sample) and $\gamma\gamma \to \pi^0$ signal. The accidental background is modeled using

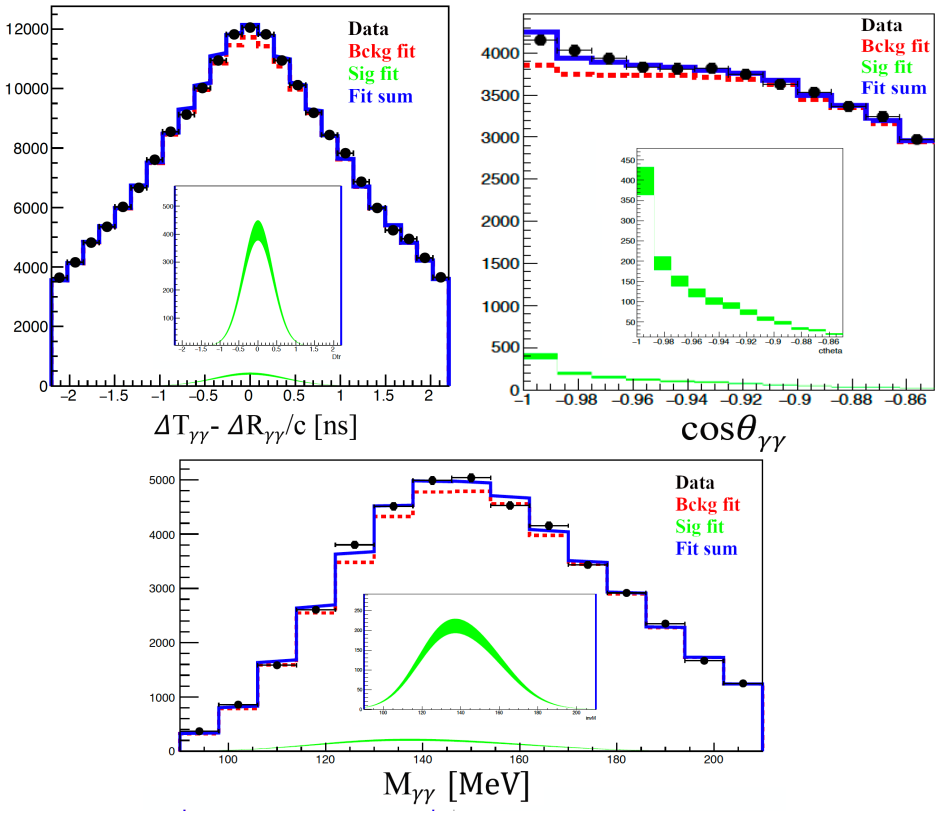


Figure 8: Simultaneous fits of the KLOE-HET coincidence sample in the $\Delta T_{\gamma\gamma} - \Delta R_{\gamma\gamma}/c$, $cos\theta_{\gamma\gamma}$ and $M_{\gamma\gamma}$ variables. Data are the black points, the accidental amount is the red dashed line, the signal is in green while the blue line is the sum of the two fits. Inserts are zooms of the signal extracted from the fit.

the HET data acquired out of coincidence window with the KLOE detector, while the $\gamma\gamma \to \pi^0$ signal is taken from the Ekhara simulation [20] interfaced with the BDSIM transport of the leptons through the beam line [21]. A carefully study of the KLOE calorimeter performance and of the KLOE trigger threshold has been performed to properly model the expected $\gamma\gamma \to \pi^0$ signal. Moreover, in the fit of the A+ sample reported in Fig. 8, the fraction of the background is fixed to the value obtained by the simultaneous fit of the accidental-pure sample.

The results shown have been obtained without considering the correlation between $P_z^{\pi^0}$ and the HET plastics. Toy MC trials, performed assuming exact signal, have been used to check the fit quality and the signal counting error reliability. The MC studies show that the error evaluation is correct, and that, the precision on $\pi^0$ counting can be further improved including in the analysis the correlation between $P_z^{\pi^0}$ and the HET scintillator position, which should increase the precision up to 6% considering the analyzed statistics and background level.

Currently, we are working to: i) measure the actual HET acceptance; ii) include the $P_z^{\pi^0}$ vs HET plastic position correlation in the analysis; ii) increase the statistics, extending the analysis to the remaining reconstructed data sample (2015-2016 data).

### 4.6 Leptophobic Dark Matter search

We conduct the search of a leptophobic mediator between Dark Matter (DM) and the SM particles, proposed in [22], using a total of 1.7 fb$^{-1}$ acquired with the KLOE detector The B-boson arises from a new $U(1)_B$ gauge symmetry that couples to the baryon number as:

$$\mathcal{L} = \frac{g_B}{3}\bar{q}\gamma^\mu q B_\mu \tag{5}$$

where $g_B$ is the $U(1)_B$ coupling, estimated to be $g_B \lesssim 10^{-2} \times (m_B/100\ \text{MeV})$. With quantum numbers $I^G(J^{PC}) = 0^-(1^{--})$, the B-boson decays in a similar way as the $\omega$-meson. It is worth noticing that the B-boson cannot be hidden under the $\rho$ meson. given the decay $B \to \pi^+\pi^-$ is forbidden by G-parity.

In KLOE the interesting region to be explored corresponds to masses below 600 MeV, where

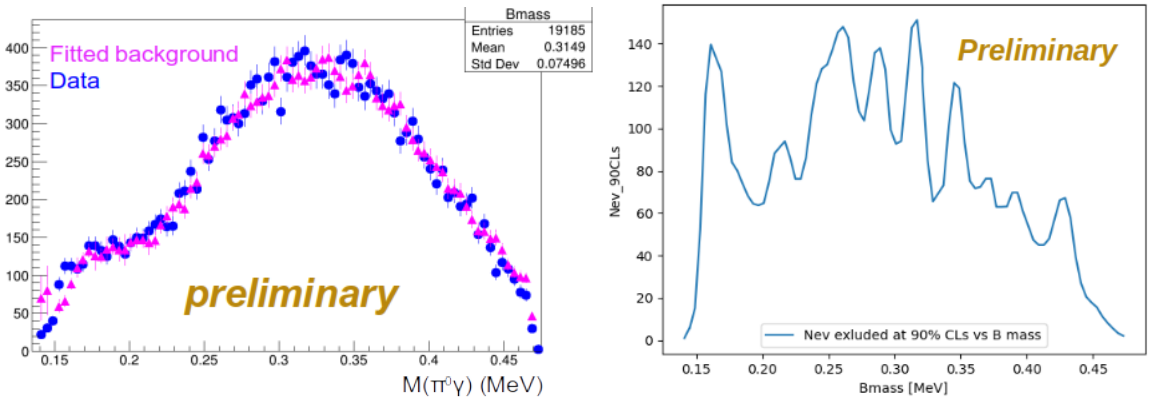


Figure 9: Left panel: Invariant mass of the $\pi^0\gamma$ system from the channel $\phi \to \eta B \to \eta\pi^0\gamma$. Blue solid dots correspond to data, magenta solid triangles are the extrapolated background from the side-bands fit. Right panel: Upper limit in the number of excluded events as a function of the B boson mass at the 90% C.L.

the dominant decay is $B \to \pi^0\gamma$ and the B-boson would appear as an enhancement in the $\pi^0\gamma$ invariant mass. In absence of a clear signal, the upper limit in the coupling of such a mediator can be established. Fig. 9 left shows the $\pi^0\gamma$ invariant mass from the decay $\phi \to \eta B$ with 1.7 fb$^{-1}$, compared to the extracted background using a side-bands fit to the data. Fig. 9 right presents the preliminary result on the upper limit as number of excluded events at 90% C.L., presented in the 59th Scientific Committee meeting.

## 5 List of Conference Talks by LNF Authors in Year 2020

1. F. Curciarello, "The KLOE-2 e$^+$ e$^-$ tagging for two-photon physics", Instrumentation for Colliding Beam Physics 2020, Novosibirsk, Russia
2. F. Curciarello, "Status of KLOE-2" Open Session talk at the 59th Scientific Committee, virtual
3. E. Perez Del Rio, "The KLOE-2 experiment at DAFNE", Conference on Flavour Physics and CP violation (FPCP) 2020, virtual
4. E. Perez Del Rio, "The KLOE-2 experiment" Open Session talk at the 60th Scientific Committee, virtual

## 6 List of Publications by LNF Authors in Year 2020

1. D. Babusci et al., "Measurement of the branching fraction for the decay $K \to \pi\mu\nu$ with the KLOE detector", Phys. Lett. B 804 (2020)
2. D. Babusci et al., "Upper limit on the $\eta \to \pi^+\pi^-$ branching fraction with the KLOE experiment", JHEP 10 (2020) 047
3. F. Curciarello for the KLOE-2 Collaboration, "The KLOE-2 $e^+e^-$ tagging for two-photon physics", Journal of Instrumentation, Volume 15, C09016 (2020)
4. E. De Lucia for the KLOE-2 Collaboration "CPT Symmetry Test at KLOE-2", J. Phys.: Conf. Ser. 1526 012006 (2020)
5. G. Bencivenni et al., "The cylindrical-GEM inner tracker detector of the KLOE-2 experiment", Nucl. Instr. and Meth. A 958, 162366 (2020)

### References


1. D. Babusci et al., Phys. Lett. B 804 (2020)
2. D. Babusci et al., JHEP 10 (2020) 047
3. D. Babusci et al., Journal of Instrumentation, Volume 15, C09016 (2020)
4. E. Perez del Rio, Acta Phys.Polon. B51 55 (2020)
5. Bernabeu, J., Di Domenico, A., Villanueva-Perez, P.: Direct test of time-reversal symmetry in the entangled neutral kaon system at a $\phi$-factory. Nucl. Phys. B868, 102–119 (2013). https://doi.org/10.1016/j.nuclphysb.2012.11.009 and Bernabeu, J., Di Domenico, A., Villanueva-Perez, P.: Probing CPT in transitions with entangled neutral kaons. JHEP 10, 139 (2015). https://doi.org/10.1007/JHEP10(2015)139
6. R.A. Bertlmann *et al.*Phys. Rev. D 60 (1999)114032; R.A. Bertlmann *et al.* Phys. Rev. A**68** (2003)012111.
7. S. Hawking, Commun. Math. Phys. 87 (1982) 395; J. Ellis *et al.* Nucl. Phys. B**241**(1984) 381; J. Ellis *et al.* Phys. Rev. D**53**(1996)3846.
8. J. Bernabeu *et al.* Phys. Rev. Lett. 92 (2004)131601; J. Bernabeu *et al.* Nucl. Phys. B**744** (2006) 180.
9. F. Ambrosino *et al.* [KLOE Coll.],Phys. Lett. B **642** (2006) 315
10. D. Babusci *et al.* [KLOE-2 Collaboration], Phys. Lett. B **730** (2014) 89
11. J. Bijnens, Phys. Scripta **T 99** 34 (2002)
12. E. Oset, J. R. Pelaez, L. Roca, Phys. Rev. **D 67** 073013 (2003)
13. B. M. K. Nefkens *et al.*, Phys. Rev. **C 90** 025206 (2014)
14. B. Di Micco *et al.*, Acta Phys. Slov. **56** 403 (2006)
15. R. R. Akhmetshin *et al.* (CMD-2 Collaboration), Phys. Lett. B **489** (2000) 125; M. N. Achasov *et al.* (SND Collaboration), Phys. Rev. D **97** (2018) 012008; J. P. Lees *et al.* (BaBar Collaboration), Phys. Rev. D **97** (2018) 052007.

16. R. R. Akhmetshin *et al.* (CMD-2 Collaboration), Phys. Lett. B **491** (2000) 81.
17. D. Babusci et al., Eur. Phys. J. C 72, 1917 (2012)
18. D. Babusci et al., Acta Phys. Pol B 46, 81 (2015)
19. R. Kleiss and H. Burkhardt, Comput. Phys. Commun. 81, 372 (1994)
20. H. Czyz, S. Ivashyn, Comput. Phys. Commun. 182 (2011)
21. I. Agapov, G.A. Blair, S. Malton, L. Deacon, Nucl. Instrum. Meth. A 606, 708 (2009)
22. S. Tulin, Phys. Rev. **D89**, 114008 (2014)